PHYSICAL REVIEW A **90**, 012507 (2014)

Ground- and excited-state properties of the polar and paramagnetic RbSr molecule: A comparative study

Piotr S. Żuchowski,[1,*] R. Guérout,[2,†] and O. Dulieu[3,‡]
[1] *Insitute of Physics, Faculty of Physics, Astronomy and Informatics, Nicolas Copernicus University, ulica Grudziadzka 5/7, 87-100 Torun, Poland*
[2] *Laboratoire Kastler-Brossel, CNRS, ENS, UPMC, Case 74, F-75252 Paris, France*
[3] *Laboratoire Aimé Cotton, CNRS, Université Paris–Sud, ENS-Cachan, Bâtiment 505, Campus d'Orsay, 91405 Orsay Cedex, France*

(Received 5 February 2014; published 9 July 2014)

This paper deals with the electronic structure of RbSr, a molecule possessing both a magnetic dipole moment and an electric dipole moment in its own frame, allowing its manipulation with external fields. Two complementary *ab initio* approaches are used for the ground and lowest excited states: first, an approach relying on optimized effective core potentials with core polarization potentials based on a full configuration interaction involving three valence electrons and second, an approach using a small-size effective core potential with 19 correlated electrons in the framework of coupled-cluster theory. We have found excellent agreement between these two approaches for the ground-state properties including the permanent dipole moment. We have focused on studies of excited states correlated to the two lowest asymptotes Rb($5p\,^2P$)+Sr($5s^2\,^1S$) and Rb($5s\,^2S$)+Sr($5s5p\,^3P$) relevant for ongoing experiments on ultracold quantum degenerate gases. We also present approximate potential curves including spin-orbit interaction based on atomic spin-orbit constants. These potential curves are an excellent starting point for experimental studies of molecular structure of RbSr using high-resolution spectroscopy.

DOI: 10.1103/PhysRevA.90.012507 PACS number(s): 31.15.A−, 67.85.−d, 31.15.vn, 34.20.Cf

I. INTRODUCTION

A detailed investigation of the properties of quantum degenerate gases of ultracold species (i.e., with kinetic energy $E_k \equiv k_B T$ equivalent to a temperature $T \ll 1$ mK) is among the most important goals of modern atomic, molecular, optical, and statistical physics. A unique feature of ultracold quantum gases is the tunability of the interaction strength between the particles with the external fields: Relying on the Feshbach resonances [1], it is possible to change the scattering length in a broad range of values. By comparison with atoms, the rich internal structure of polar molecules (i.e., possessing a permanent electric dipole moment) and their mutual strong anisotropic interactions can offer to this field novel opportunities for precise tests of fundamental theories and for quantum control using electromagnetic fields [2,3]. Ultracold molecules trapped in periodic optical lattices have been proposed as qubits for prototypes of quantum computers [4] or as quantum simulators for studies of many-body phenomena such as phase transitions, strongly correlated systems, or many-body physics in reduced dimensions [5,6]. In 2008 two groups reported the formation of ultracold gases of polar LiCs and KRb molecules in ultracold temperatures [7,8]: Ultracold LiCs molecules were obtained by photoassociation of pairs of ultracold Li and Cs atoms and spontaneous decay of excited LiCs* molecules down to the electronic ground state, while ultracold KRb molecules have been created through magnetoassociation of ultracold K and Rb atoms into weakly bound levels of the molecular ground state, followed by stimulated Raman adiabatic passage (STIRAP) toward the lowest rovibrational level [8,9]. There are also a number of other experiments aiming at creating ultracold heteronuclear diatomic alkali-metal molecules in their ground state such as RbCs [10,11] and NaK [12], since in contrast to KRb [13] they are stable with respect to the chemical reactions of atom exchange and trimer formation [14].

Heteronuclear diatomic alkali-metal molecules in their ground state $X\,^1\Sigma^+$, however, are not easy to manipulate with external fields: Their very weak magnetic moment originates only from nuclear spin and they do not exhibit a linear Stark effect in the rovibrational ground state. A very interesting class of quantum simulators has been proposed by Micheli *et al.* [5] employing molecules with both an electric and a magnetic dipole moment in their own frame. Such molecules reveal fascinating potential for high-precision measurements (for example, the YbF molecule is being used in the determination of bounds for the electric dipole moment of the electron [15]) or for sensitive imaging of low-frequency electromagnetic fields [16]. In the rest of the paper we will qualify in short such species as paramagnetic and polar molecules.

Possible candidates for paramagnetic and polar molecules are diatomic molecules formed by association of laser-coolable atoms with different atomic spin quantum numbers, such as pairs of alkali-metal atoms and alkaline-earth atoms [17,18]. One of the most promising candidates for such a system is the RbSr molecule. Besides its magnetic doublet $X\,^2\Sigma^+$ electronic ground state, it exhibits a permanent electric dipole moment of 1.4–1.5 D [17,18]. The laser cooling, trapping, and manipulation of Rb atoms were well established at the very beginning of the ultracold matter studies [19]. At present the strontium atom is one of the most popular atomic species in ultracold physics [20,21]: For example, studies of Bose-Einstein condensation of Sr atoms and Bose-Fermi mixtures (of different Sr isotopes) have recently been reported [22–26]. Moreover, a STIRAP scheme has been developed to produce weakly bound Sr_2 molecules in the ground electronic state [23]. It is finally worth mentioning that Sr_2 molecules have also been produced by spontaneous decay from the

---

[*] pzuch@fizyka.umk.pl
[†] romain.guerout@spectro.jussieu.fr
[‡] olivier.dulieu@u-psud.fr

excited Sr(^1S)-Sr($^3P_1$) molecular state [27]. More recently, a quantum degenerate gas of rubidium atoms coexisting with strontium has been produced [28]. Another motivation that makes the study of the RbSr system particularly interesting is the magnetic tunability of the scattering length due to the presence of subtle mechanisms that can produce the Feshbach resonances [18]. That might allow the experimentalist to modify the scattering length in the ultracold mixture of Rb and Sr and control the behavior of a quantum gas of such atoms. It is worth mentioning that several other similar species are subject to intense ongoing research, such as YbLi [29–33] and YbRb [34–36].

Manipulation of the quantum states of diatomic molecules with laser light requires the knowledge of appropriate transition energies and thus of the potential energy curves (PECs) supporting the relevant energy levels and the corresponding transition dipole moments (TDMs). Surprisingly enough, still only little is known about the structure of molecules containing alkali-metal atoms with group II atoms. The electronic structure of Ba neutral compounds (BaLi, BaNa, and BaK) has been explored some time ago by Allouche and co-workers [37–39]. Other studies concern CaLi [40–42] and LiBe [43,44]. More recently, the electronic structures of the related molecular ions containing one alkali-metal atom and Ca^+ [45], Sr^+ [46], or Ba^+ [47–50] with various high-level approaches have been published in relation to experiments aiming at creating cold molecular ions in merged cold ion and cold atom traps.

In this paper we present a study of interactions of Rb and Sr atoms in ground and excited states. We recently examined this system in its $X\,^2\Sigma^+$ ground state with two entirely different approaches [17,18]: One relies on the representation of RbSr as a three-valence-electron molecule in the field of relativistic polarizable large effective core potentials (ECPs) through a full configuration-interaction (FCI) calculation, while the other treats explicitly 19 electrons in the field of a relativistic small core ECP via the coupled-cluster (CC) theory. Here we use these approaches to revisit and extend the study of the electronic structure of the RbSr system. The methods are described in Sec. II. The ground-state properties of RbSr are carefully revisited in Sec. III including the potential curve, the permanent dipole moment, and the static dipole polarizability. We have calculated the PECs and the transition dipole moments between the $X\,^2\Sigma^+$ [Rb($5s\,^2S$)+Sr($5s^2\,^1S$)] ground state and the excited $^2\Sigma^+$ and $^2\Pi^+$ states correlated to the two lowest asymptotes Rb($5p\,^2P$)+Sr($5s^2\,^1S$) and Rb($5s\,^2S$)+Sr($5s5p\,^3P$) relevant for the ongoing experiments (Sec. IV). We have also investigated the spin-orbit (SO) coupling of these states within the framework of an atomic model involving experimental atomic SO splittings. The results of this paper are of key importance in experimental investigations of the spectroscopy and dynamics of the RbSr diatom. These data could be adjusted to spectroscopic data in order to provide the essential information for designing optical routes for the formation of ultracold ground-state RbSr molecules in their lowest internal level, thus leading toward a degenerate quantum gas of molecules with both magnetic and electric dipole moments. In the rest of the paper, atomic units for distances (1 a.u. $= a_0 = 0.052\,917\,7$ nm), energies ($E_h = 1$ a.u. $= 2R_\infty = 219\,474.631\,37$ cm^{-1}), and dipole moment (1 a.u. $= 2.541\,580\,59$ D) will be used, except otherwise stated. The potential energy curves obtained in this paper are provided in Ref. [51].

II. METHODS

The first method is identical to the one used in our previous works for $RbSr^+$ [46] and for the RbSr ground state [17]. It is based on the representation of the Rb^+ and Sr^{2+} ionic cores by a relativistic ECP complemented with a core polarization potential (CPP) simulating the core-valence correlation along the lines developed by Müller *et al.* [52,53] and Foucrault *et al.* [54]. These effective potentials involve semiempirical parameters (reported in Ref. [17]), which are chosen to reproduce the energies of the lowest s, p, and d levels of the Rb and Sr^+ one-valence-electron systems. A FCI method involving three valence electrons is performed in the framework of the configuration interaction by perturbation of a multiconfiguration wave function selected iteratively (CIPSI) method developed at Paul Sabatier University in Toulouse, France. From now on we will refer to this method as FCI–ECP+CPP. Previous works on alkali-metal dimers (see, for instance, Refs. [55–57]) have demonstrated that this approach yields results for equilibrium distances R_e and potential well depths D_e for ground and excited states in good agreement with those obtained from experiments: For example, the discrepancy on D_e for the $^1\Sigma^+$ ground states of alkali-metal dimers is typically much less than 100 cm^{-1}, often (e.g., for KRb) less than 20 cm^{-1}. Values for permanent electric dipole moments (PEDMs) of their $^1\Sigma^+$ ground state [55] match those measured in recent ultracold molecule experiments (e.g., for KRb [8] and LiCs [58]). The TDM functions are also found in close agreement with other theoretical values [56,59,60]. The (well-known) main advantage of the FCI–ECP+CPP method is its versatility and robustness: Several low-lying excited states can be easily calculated regardless of their total spin, in contrast to the single-reference quantum chemistry methods we employ in this paper. Among the disadvantages is its rapid increase of computational cost with increased basis-set size. Just as in Ref. [17], the basis set used in these calculations was limited to s, p, and d Gaussian-type basis functions, which translates into a number of configurations of about 10^5. In the present case, the lack of f orbitals mostly affects the evaluation of the dispersion interaction, i.e., its dependence on R^{-6} is well reproduced, but its magnitude may not be correct. The basis-set superposition error (BSSE) has not been introduced, as we have checked that it remains small (less than 1 cm^{-1}) for the three valence electrons, while it is hard to estimate for the core electrons, which are not explicitly taken in account.

The second method involves the calculations with the fully relativistic small-core ECP referred to as ECP28MDF obtained by Lim *et al.* [61,62], such that all $4s$, $4p$, and $5s$ electrons (19) of Rb and Sr are correlated on both atoms. The PECs for the $X\,^2\Sigma^+$ ground state and for the lowest quartet Σ^+ and Π states are determined within the open-shell spin-restricted coupled-cluster (RCC) theory [63] with single, double, and triple excitations [RCCSD(T)] as in Ref. [18] implemented in the MOLPRO 2012 package [64]. In comparison to this work, we performed the calculations with a significantly improved basis set in order to estimate the error attributed to the basis-set

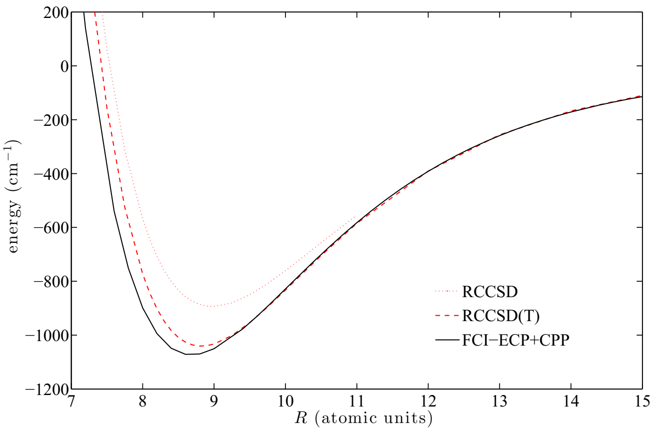

FIG. 1. (Color online) The RbSr ground-state potential energy curves obtained with the RCCSD (dotted red line), RCCSD(T) (dashed red line), and FCI–ECP+CPP methods (solid black line).

incompleteness. We used the original uncontracted basis sets of Lim *et al.* [61,62], to which we have added d, f, and g Gaussian-type basis functions to improve the core-valence correlation between the $4s$ and $4p$ shells with the $5s$ one. We also added a series of diffuse $spdfg$ basis functions using an even tempered scheme to better describe the dispersion interaction. We have further added $3s3p3d2f2g$ bonding functions. We label this new basis set with its maximum angular momentum $l_{\max} = 4$. We have further extended this set to build a new one (labeled by $l_{\max} = 5$) including one more large-exponent g function for the core-valence correlation and one diffuse h function. The latter has been used only for ground-state calculations. Both basis sets can be found in Ref. [51].

The doublet excited states have been obtained with the spin-restricted version of the open-shell equation-of-motion coupled-cluster method limited to singly and doubly excited configurations (EOM-CCSD) [65,66] implemented in the CFOUR package [67]. This approach allows for calculating excitation energies from the electronic ground state to the excited state of any spatial symmetry, but it is unable to calculate the spin-flip transitions (and thus those involving the quartet states). The excitation energies of doublet states obtained with the EOM-CCSD method were then added to the ground-state potential energy curve, while the lowest $1\,^4\Sigma^+$ and $1\,^4\Pi$ PECs were shifted in order to smoothly match the Rb($5s\,^2S$)+Sr($5s5p\,^3P$) asymptotes calculated with the EOM-CCSD method. The basis functions were restricted to the $l_{\max} = 4$ set with removed bonding functions.

III. GROUND-STATE PROPERTIES OF RbSr

We present the results of our electronic-structure calculations for the ground-state RbSr dimer using the RCCSD(T) method with both basis sets above in order to investigate the discrepancies between the spectroscopic parameters obtained by Guérout *et al.* [17] and Żuchowski *et al.* [18] and to estimate the error bars due to the basis-set truncation in CC calculations. The results are shown in Fig. 1, while the essential spectroscopic parameters are gathered in Table I.

TABLE I. Equilibrium distance R_e (in a_0) and potential depth D_e (in cm^{-1}) of the RbSr ground state obtained by the various approaches discussed in the text.

Method	R_e (units of a_0)	D_e (cm^{-1})
FCI–ECP+CPP[a]	8.69	1073.3
RCCSD(T)[b]	8.86	999.6
	$l_{\max} = 4$ basis set	
RCCSD	8.99	885.6
RCCSD(T)	8.83	1034.4
UCCSD	8.99	898.5
UCCSD(T)	8.81	1052.5
	$l_{\max} = 5$ basis set	
RCCSD	8.98	893.6
RCCSD(T)	8.82	1040.5
UCCSD	8.97	896.7
UCCSD(T)	8.80	1059.1

[a] Reference [17].
[b] Reference [18].

The ground-state potential calculated with the FCI–ECP+CPP method [17] is $D_e = 1073.3$ cm^{-1} deep with an equilibrium distance $R_e = 8.69a_0$, while in Ref. [18] the depth of the RbSr potential was found to be equal to 1000 cm^{-1} at $R_e = 8.86a_0$. With the new basis sets we have found that D_e is approximately 3%–4% larger: The RCCSD(T) value is increased to $D_e = 1034.4$ cm^{-1} with the $l_{\max} = 4$ basis set and to $D_e = 1040.5$ cm^{-1} with the $l_{\max} = 5$ one. The difference in D_e in these basis sets is most likely related to a saturation of the dispersion energy in the calculations involving Gaussian functions. Based on the well-known behavior of the correlation energy as a function of the maximum angular momentum in the basis set [68], we can deduce the complete basis limit expected for the RCCSD(T) method, yielding a total interaction energy 1047.9 cm^{-1}. In fact, it is reasonable to treat the difference between the extrapolated result and the interaction energy calculated using the $l_{\max} = 5$ basis set as the uncertainty of the calculation. It is still quite hard to estimate the error beyond the RCCSD(T) calculation and to this end we will compare how an analogous methodology performs for the Sr_2 and singlet Rb_2 molecules. Skomorowski *et al.* have shown [69] that the CCSD(T) dissociation energy of the Sr_2 dimer (1124 cm^{-1}), calculated with the same core potential and a similar basis set, is slightly larger (by 3.8%) than the experimental dissociation energy (1082 cm^{-1}). The well depth of the Rb_2 ground-state CCSD(T) PEC obtained with the ECP and basis set used in present study underestimates the experimental value (3836 cm^{-1}) by 6%. Thus, taking a 5% uncertainty (52 cm^{-1}) on our potential is certainly a conservative estimate. For completeness, we have also calculated the RbSr ground-state PEC with spin-unrestricted coupled-cluster (UCC) approach: The potential depth for the UCCSD(T) approach is no more than 20 cm^{-1} larger than in the restricted case, which is within the estimated error bound.

The result from the FCI–ECP+CPP calculation falls within such an error bound, as the well depth is only 33 cm^{-1} deeper than the RCCSD(T) value. The agreement between harmonic constants ω_e is also very good: 38.98 cm^{-1} with the FCI–ECP+CPP approach and 38.09 cm^{-1} with the RCCSD(T)

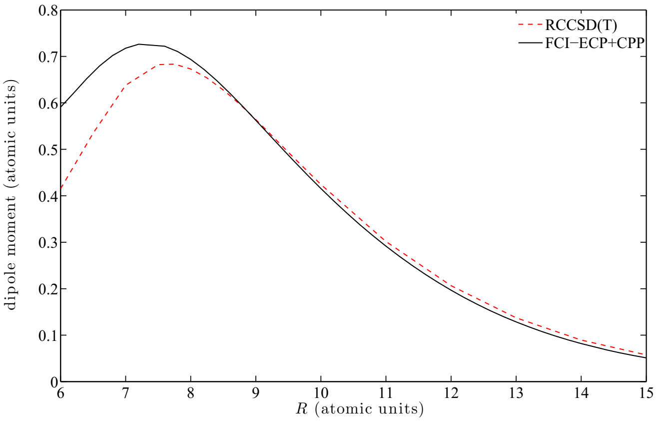

FIG. 2. (Color online) Permanent electric dipole moment of the RbSr ground state calculated with the finite-field method through the RCCSD(T) (dashed red line) and the FCI–ECP+CPP approach [17] (solid black line).

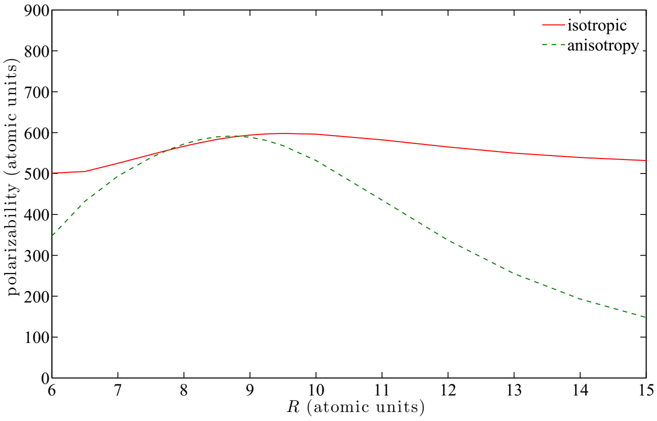

FIG. 3. (Color online) Isotropic static dipole polarizability and the corresponding anisotropy of the RbSr ground state calculated with the finite-field RCCSD(T) method.

calculations and the $l_{\max} = 5$ basis set. Note, however, that R_e is smaller by about $0.1a_0$ in the FCI–ECP+CPP approach than in the RCCSD(T) approach.

In fact, both curves differ by merely one bound state and further two-color photoassociation spectroscopy for several isotopic mixtures of RbSr should provide the exact number of bound states supported by the RbSr potential. The potential energy curves reported in this paper should be an excellent starting point for refinement using the experimental data.

Other properties of the RbSr ground state reveal the present quality of the electronic wave function when the results are compared between the two methods. Figure 2 displays the ground-state PEDM functions computed within the finite-field approach, as obtained with the FCI–ECP+CPP method [17], and the present RCCSD(T) computation with an extended basis set. Both approaches yield very similar variation and magnitude and thus very similar electronic wave functions. At the equilibrium distance the PEDMs are almost identical (1.54 D) and they become slightly different only at short internuclear distances. Note that with previously reported calculations [18], with the RCCSD(T) method employing a smaller basis set, the value of the dipole moment was found to be 1.36 D.

A similar finite-field approach allows for calculating the static dipole polarizability of the RbSr ground state as the second derivative of the RCCSD(T) energy with respect to the amplitude of an external electric field. We display in Fig. 3 the R-dependent isotropic polarizability α_0 and the corresponding anisotropy $\Delta\alpha$, which are related to the Cartesian components according to the well-known formula

$$\alpha_0 = \tfrac{1}{3}(2\alpha_{xx} + \alpha_{zz}), \quad \Delta\alpha = \alpha_{zz} - \alpha_{xx}. \tag{1}$$

For the equilibrium distance the anisotropy of polarizability of the RbSr molecule and the averaged polarizability are almost equal. The anisotropic polarizability peaks near R_e, while α_0 has its maximum for $9.6a_0$. The anisotropy $\Delta\alpha$ at the equilibrium distance is very large and comparable to the largest anisotropies reported for alkali-metal dimers [7,70–72]. With the large dipole moment and the large anisotropy of polarizability of RbSr, the RbSr molecule can be considered a good candidate for manipulation with intense off-resonant laser light [73–75].

IV. EXCITED STATES OF THE RbSr MOLECULE

Figure 4 shows a diagram of the excited energy levels of Rb and Sr and lists the related Hund's (a) case states of RbSr. From the experimental point of view, the most interesting excited states are those correlating with the lowest asymptotes Rb(^2S)+Sr($^3P_{0,1,2}$) and Rb(^2P)+Sr(^1S). In particular, the forbidden transition $^1S \rightarrow {}^3P_1$ in the Sr atom is very appealing for photoassociation experiments and optical manipulation due to its narrow width. This intercombination line has also been

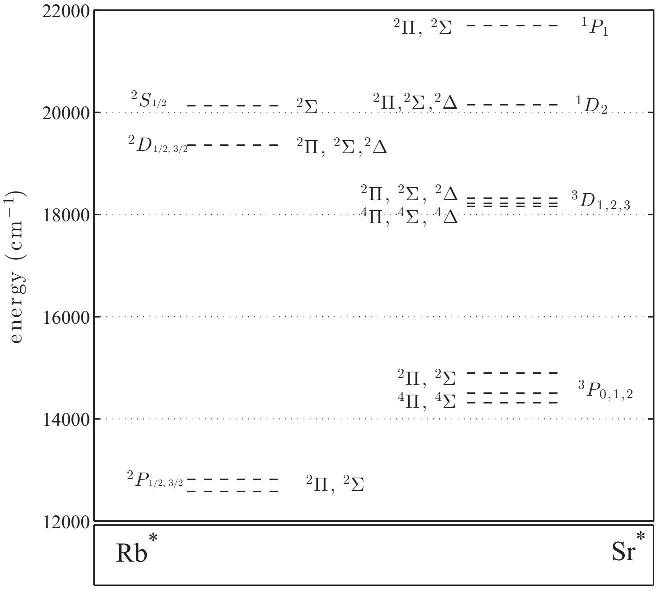

FIG. 4. Experimental excited energy levels of Rb and Sr atoms featuring the corresponding dissociation limits (adding a ground-state Sr atom on the left column and a ground-state Rb atom on the right column) of the molecular Hund's (a) case states of the RbSr molecule. The Rb $^2D_{3/2,5/2}$ energies of Rb are identical within the resolution of the plot. The origin of energies corresponds to infinitely separated ground-state Sr and Rb atoms.

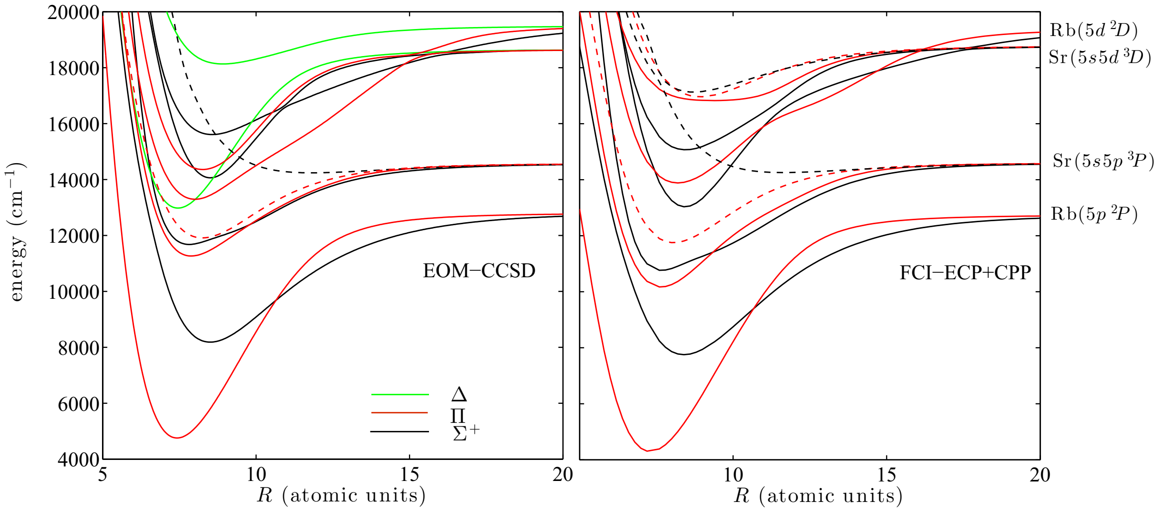

FIG. 5. (Color online) Hund's case (a) potential energy curves of the excited RbSr molecule obtained with the EOM-CCSD method (left panel) and the FCI–ECP+CPP method (right panel). Dashed lines denote the quartet states, while the doublet states are plotted with solid lines.

used recently for the creation of ground-state Sr_2 molecules [23,27] and for optical tuning of the Sr scattering length [76–78]. We have also found that the states correlated to the Rb(^2S)+Sr(^3P) asymptote might interact with higher excited states, thus we have also explored a few of them, namely, the states correlated to Rb(^2S)+Sr(^3D) and Rb(^2D)+Sr(^1S) asymptotes that are separated only by about 1000 cm^{-1}. Note that the Rb($6s\,^2S$) and the Sr($5s4d\,^1D$) levels are very close to each other (20 132.5 and 20 149.7 cm^{-1}), so the *ab initio* calculations are very difficult to perform, regarding especially the proper order of the asymptotic molecular states. The present approaches, however, have been successful in this matter. The excited-state PECs calculated with both methods presented in Sec. II are displayed in Fig. 5, while in Table II we report the main spectroscopic parameters of the Hund's case (a) PECs correlated to Rb(^2S)+Sr($^3P_{0,1,2}$) and Rb(^2P)+Sr(^1S).

A. The Rb($5p\,^2P$)-Sr(^1S) interaction

The two RbSr Hund's (a) case states correlated to this limit are denoted by $2\,^2\Sigma^+$ and $1\,^2\Pi$. By construction the FCI–ECP+CPP method involves the exact asymptotic energy of 12 737 cm^{-1} (deduced from the position of P-state multiplet and Landé rule), while the EOM-CCSD method yields 12 793 cm^{-1}, in good agreement (better than 0.5%) with the former value. The overall agreement for the main spectroscopic quantities between the FCI–ECP+CPP and EOM-CCSD PEC methods is satisfactory (see Table II). Just like for the ground-state PEC, the FCI–ECP+CPP method gives equilibrium distances shorter by about $0.1a_0$ compared to the EOM-CCSD ones. The well depths are deeper by about 5%–7% and the harmonic constants are smaller by about 5% compared to the EOM-CCSD results. Note that both methods place the crossing between the $^2\Sigma^+$ and $^1\Pi$ states at almost the same distance: $10.67a_0$ in the case of the FCI–ECP+CPP method and $10.65a_0$ for the EOM-CCSD method.

Very good agreement is found between the two methods on the PEDM of both the $2\,^2\Sigma^+$ and $1\,^2\Pi$ states [Fig. 6(a)], demonstrating again that both methods indeed yield very similar electronic wave functions. The positions of the maximum values of the PEDMs agree within $0.1a_0$, whereas their (large) magnitudes at this point agree to better than 5%. The existence of two maxima in the $2\,^2\Sigma^+$ PEDM is probably related to a sudden change of chemical character of the RbSr molecule near the repulsive wall into an ion-pair state. As can be expected from the previous results on PEDMs, the agreement on the TDM functions for these states [Fig. 7(a)] is also excellent between the two approaches, as they involve

TABLE II. Main spectroscopic parameters of the lowest excited states of the RbSr Hund's case (a) potential energy curves.

	FCI ECP+CPP			EOM-CC			
State	R_e (units of a_0)	D_e (cm^{-1})	ω_e (cm^{-1})	R_e (units of a_0)	D_e (cm^{-1})	ω_e (cm^{-1})	Asymptote
$1\,^2\Sigma^+$	8.69	1073.3	38.98	8.82	1040.5	38.09	Rb($5s\,^2S$)+Sr(^1S)
$2\,^2\Sigma^+$	8.40	4982.9	58.37	8.51	4609.6	60.20	Rb($5p\,^2P$)+Sr(^1S)
$3\,^2\Sigma^+$	7.67	3828.0	65.26	7.81	2892.4	62.48	Rb($5s\,^2S$)+Sr($5s5p\,^3P$)
$1\,^2\Pi$	7.31	8439.8	79.50	7.42	8038.6	83.19	Rb($5p\,^2P$)+Sr(^1S)
$2\,^2\Pi$	7.65	4421.2	67.60	7.88	3303.5	63.37	Rb($5s\,^2S$)+Sr($5s5p\,^3P$)
$1\,^4\Sigma^+$	11.63	336.3	15.42	11.81	329.2	15.03	Rb($5s$)+Sr($5s5p\,^3P$)
$1\,^4\Pi$	8.06	2838.1	56.98	8.24	2655.7	54.95	Rb($5s$)+Sr($5s5p\,^3P$)

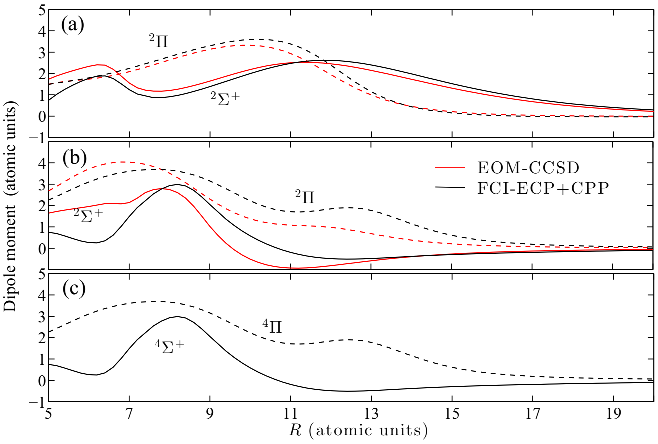

FIG. 6. (Color online) Permanent electric dipole moments for (a) the $2\,^2\Sigma^+$ and $1\,^2\Pi$ states correlated to Rb($5p\,^2P$)-Sr($5s\,^1S$), (b) the $3\,^2\Sigma^+$ and $2\,^2\Pi$ states correlated to Rb($5s\,^2S$)+Sr($5s5p\,^3P$), and (c) the $1\,^4\Sigma^+$ and $1\,^4\Pi$ states correlated to Rb($5s\,^2S$)+Sr($5s5p\,^3P$), calculated with the FCI–ECP+CPP and EOM-CCSD approaches. The solid lines denote $^{2,4}\Sigma^+$ symmetry and the dashed lines the $^{2,4}\Pi$ symmetry.

ground- and excited-state wave functions, which are represented in almost identical ways. Note that the asymptotic limit of these TDMs (3.013 a.u.) calculated at very long range agrees very well with the experimental atomic value $^2S \rightarrow {}^2P_{1/2}$ transition (2.99 a.u.). At short distances the $X\,^2\Sigma^+ \rightarrow 1\,^2\Pi$ transition is clearly favored with respect to the $X\,^2\Sigma^+ \rightarrow 2\,^2\Sigma^+$ transition.

B. The Rb($5s\,^2S$)-Sr($5s5p\,^3P$) interaction

Four Hund's case (a) molecular states are correlated to this asymptote, which are denoted by $3\,^2\Sigma^+$, $1\,^4\Sigma^+$, $2\,^2\Pi$, and $1\,^4\Pi$. All four states can easily be calculated with the FCI–ECP+CPP approach, while the computing codes for the open-shell EOM-CCSD method for spin-changing states are not available. As mentioned in Sec. II, the $1\,^4\Sigma^+$ and $1\,^4\Pi$ quartet states correlating with Rb(^2S)+Sr(^3P) are the lowest ones for the given spatial and spin symmetries and are dominated by a single electronic configuration so that their PECs can be obtained with the RCCSD(T) method.

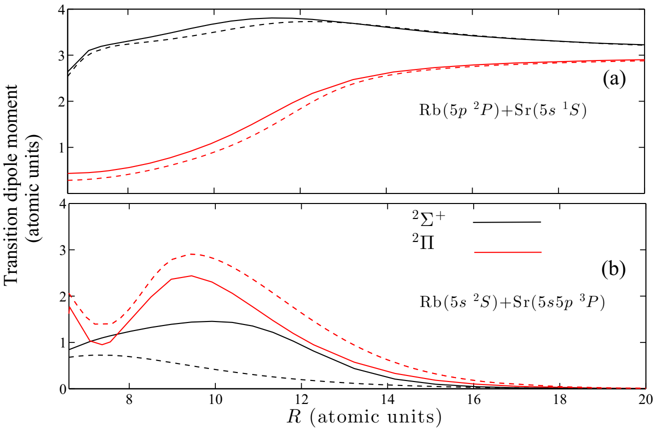

FIG. 7. (Color online) Transition dipole moments from the RbSr ground state $X\,^2\Sigma^+$ towards (a) the $2\,^2\Sigma^+$ state (black lines) and the $1\,^2\Pi$ (red lines) state and (b) the $3\,^2\Sigma^+$ state (black lines) and the $2\,^2\Pi$ (red lines) state, obtained with the EOM-CC (solid lines) and FCI–ECP+CPP methods (dashed lines).

The asymptotic limit of the excitation energies obtained for these states is correctly reproduced to better than 1% by our calculations when compared to the experimental value 14 705 cm^{-1} deduced from atomic data through the Landé rule for the ^3P strontium multiplet. The FCI–ECP+CPP method yields 14 615 cm^{-1} [17] by construction for both the quartet and doublet states. The EOM-CCSD value for doublet states is 14 567.8 cm^{-1}.

Being the lowest states of their symmetry, the main spectroscopic constants for the $1\,^4\Sigma^+$ and $1\,^4\Pi$ PECs show good agreement between the two methods, similar to that obtained for the ground-state PEC (Table II). In contrast, we immediately see from the table and from Fig. 5 that larger discrepancies are found between the two methods for doublet states. The equilibrium distance is now shorter by about $0.2a_0$ in the FCI–ECP+CPP method. While consistent in magnitude, the harmonic constants differ by about 4 cm^{-1} between the two methods. The largest discrepancy concerns the well depth of the $3\,^2\Sigma^+$ and $2\,^2\Pi$ states, which is deeper by about 1000 cm^{-1} in the FCI–ECP+CPP results. The PEDM functions of Fig. 6(b) reveal that while having similar trends, the details of the electronic wave functions induce significant differences in the oscillating patterns, i.e., in the relative weights of the configurations. Obviously this feature transfers into the TDM functions of Fig. 7(b), in particular for the $X\,^2\Sigma^+ \rightarrow 3\,^2\Sigma^+$ transition where the magnitude of the TDM is weaker by about a factor of 2 in the FCI–ECP+CPP results compared to the EOM-CC ones, probably related to the different position of the node visible in the $3\,^2\Sigma^+$ PEDM. Nevertheless, these TDMs deserve more attention. Asymptotically such transitions are in principle forbidden due to atomic spin-flip selection rule. Actually, the $^1S \rightarrow {}^3P_1$ excitation is allowed by the electric dipole transition due to second-order spin-orbit mixing with the higher $^1P_1$ state, while the excitation towards the $^3P_{0,2}$ states is strongly forbidden. In the molecular region, the disallowed transition from the ground state becomes allowed due to the Pauli exchange interaction, which can be measured by the magnitude of the exchange energy [79]). The quite sudden increase of the TDM around $15a_0$ reflects the exponential variation of this exchange energy when the valence-overlap region is reached.

Further studies with the EOM-CC method that includes triply excited clusters and all-electron relativistic studies could probably help validate one of these results. Note that in the FCI–ECP+CPP approach the $1\,^4\Pi$ state is well separated in energy from other states to which it is coupled by the spin-orbit interaction (see the next section), while it crosses the doublet states in the EOM-CC method. If the former result would be confirmed, this means that strongly polar metastable RbSr molecules could be created and used for further manipulation in the experiments.

C. Higher excited states

Higher excited states of RbSr cannot be disregarded in the present analysis. An inspection of Fig. 5 shows that the $3\,^2\Pi$ and $4\,^2\Sigma^+$ PECs correlated to the Rb($5s\,^2S$)+ Sr($5s4d\,^3D$) dissociation limit are submerged below the Rb($5s\,^2S$)+Sr($5s5p\,^3P$) asymptote by several hundreds of cm^{-1} in both methods. The bottom of the well of the $1\,^2\Delta$ state (computed with the EOM-CCSD approach) is submerged by more than 1000 cm^{-1} below that asymptote. Moreover, due to the proximity of their asymptotes, the excited states that correlate with Rb($4d\,^2D$)+Sr($5s^2\,^1S$), Rb($5s\,^2S$)+Sr($5s4d\,^3D$), and Rb($5s\,^2S$)+Sr($5s4d\,^1D$) strongly mix together and exhibit numerous avoided crossings that are consistently predicted by both methods: around $16a_0$ for the $^2\Pi$ states and around $16a_0$ (EOM-CCSD) or $18a_0$ (FCI–ECP+CPP) for the $^2\Sigma^+$ states. Both approaches also predict the presence of short-range avoided crossings of Π and Σ^+ states but with more more pronounced differences in positions. Finally, we observe the large difference in the potential wells depths for Π and Σ^+ states correlated to Rb($4d\,^2D$)+Sr($5s^2\,^1S$) and Rb($5s\,^2S$)+Sr($5s4d\,^3D$).

D. Long-range behavior close to the Rb($5p\,^2P$)+Sr($5s^2\,^1S$) and Rb($5s\,^2S$)+Sr($5s5p\,^3P$) asymptotes

We have obtained the C_6 values for the excited states by fitting the calculated potential energy curves at long range to the C_6R^{-6} analytic form. This procedure has to be performed very carefully: Backing out the van der Waals coefficients from the potential energy curves needs very-high-precision potential energy curves for a broad range of distances. As invoked in Sec. II, due to the lack of high angular momentum functions in the basis set used in the FCI–ECP+CPP computations, we performed such fittings only for the CC methods. For the doublet states correlated to the Rb($5p\,^2P$)+Sr($5s^2\,^1S$) limit we obtained $C_6(2\,^2\Sigma^+) = 23324E_ha_0^6$ and $C_6(1\,^2\Pi) = 8436E_ha_0^6$ compared to the values of Ref. [80], $17\,530E_ha_0^6$ and $8331E_ha_0^6$, respectively. Despite the nice agreement obtained for the latter value, error bars for these values can be large and unpredictable as these values were obtained by fitting to the shape of the EOM-CCSD potential energy curve added to the ground-state interaction energy of RbSr. In contrast, the C_6 values for the excited states correlating with Rb($5s\,^2S$)+Sr($5s5p\,^3P$) can be extracted with much better accuracy since for the quartet states potential energy curves are obtained in a direct way and not as a sum of the interaction energy plus EOM-CC excitation. We obtained $C_6(2\,^2\Sigma^+) = 5265E_ha_0^6$ and $C_6(1\,^2\Pi) = 4654E_ha_0^6$, which are in satisfactory agreement with the values $5735E_ha_0^6$ and $5000E_ha_0^6$ of Ref. [80].

E. Relativistic picture of the lowest excited states of RbSr

Spin-orbit splittings are quite large for the lowest excited states of both atoms: 237.6 cm^{-1} for Rb($5p\,^2P$) and 581.1 cm^{-1} for Sr($5s5p\,^3P$). Therefore, they must be taken into account in any accurate representation of the RbSr excited states for the purpose of modeling experimental results. It is well known that, due to configuration mixing, the SO couplings vary with the internuclear distance and can be reduced or enhanced typically by 30%–50% compared to the atomic values. Examples can be found, for instance, in spectroscopic studies of RbCs [81] or KCs [60] or in quantum chemistry studies of Sr_2 [82], SrYb [83], or Rb_2 [84]. It is beyond the goal of this paper to compute the R dependence of the SO coupling in RbSr. Instead we present an approximate model where the atomic SO is used as a perturbation to the Hund's case (a) states [85] in order to deliver a preliminary picture of the relevant PECs. Due to the large energy separation of the Rb($5p\,^2P$)+Sr(^1S) and Rb($5s\,^2S$)+Sr($5s5p\,^3P$) asymptotes, the corresponding manifold of PECs can safely be considered as isolated from each other. We will also ignore the higher excited states discussed above, which are submerged below the Rb($5s\,^2S$)+Sr($5s5p\,^3P$) asymptote.

We follow the usual spectroscopic convention and use the symbols Λ and Σ for the projection onto the molecular axis of the electronic quantities, namely, the orbital angular momentum and the spin, respectively, and $\Omega = |\Lambda + \Sigma|$. The atomic SO constants are $A_{\text{Rb}} = \Delta E_{\text{fs}}[\text{Rb}(5p\,^2P)]/3 = 79.2\ \text{cm}^{-1}$ and $A_{\text{Sr}} = \Delta E_{\text{fs}}[\text{Sr}(5s5p\,^3P)]/3 = 193.7\ \text{cm}^{-1}$. We use the fact that the matrix elements of the spin-orbit Hamiltonian $H_{\text{SO}} = A\mathbf{L}\cdot\mathbf{S}$ in the basis $|SL\Sigma\Lambda\rangle$ can be expressed in the *asymptotic* basis set of atomic angular momenta using Clebsch-Gordon coefficients

$$|SL\Sigma\Lambda\rangle = \sum_{\Sigma_{\text{Rb}},\Sigma_{\text{Sr}}} \langle S_{\text{Rb}}\Sigma_{\text{Rb}}S_{\text{Sr}}\Sigma_{\text{Sr}}|S\Sigma\rangle |S_{\text{Rb}}\Sigma_{\text{Rb}}\rangle |S_{\text{Sr}}L\Sigma_{\text{Sr}}\Lambda\rangle, \tag{2}$$

which more specifically reduces for doublet states to

$$\left|\tfrac{1}{2}L \pm \tfrac{1}{2}\Lambda\right\rangle = \pm\sqrt{\tfrac{1}{3}}\left|\tfrac{1}{2}\,\tfrac{1}{2}\right\rangle_{\text{Rb}}|1L0\Lambda\rangle_{\text{Sr}} \mp \sqrt{\tfrac{2}{3}}\left|\tfrac{1}{2}-\tfrac{1}{2}\right\rangle_{\text{Rb}}|1L1\Lambda\rangle_{\text{Sr}}, \tag{3}$$

while for the quartet states it reads

$$\left|\tfrac{3}{2}L \pm \tfrac{1}{2}\Lambda\right\rangle = \sqrt{\tfrac{1}{3}}\left|\tfrac{1}{2}\,\tfrac{1}{2}\right\rangle_{\text{Rb}}|1L0\Lambda\rangle_{\text{Sr}} + \sqrt{\tfrac{2}{3}}\left|\tfrac{1}{2}-\tfrac{1}{2}\right\rangle_{\text{Rb}}|1L1\Lambda\rangle_{\text{Sr}}, \tag{4}$$

$$\left|\tfrac{3}{2}L \pm \tfrac{3}{2}\Lambda\right\rangle = \left|\tfrac{1}{2} \pm \tfrac{1}{2}\right\rangle_{\text{Rb}}|1L \pm 1\Lambda\rangle_{\text{Sr}}. \tag{5}$$

The interaction of the rubidium atom in the ^2P state with the Sr ground-state atom splits the degeneracy of the ^2P state into $^2\Sigma^+$ and $^2\Pi$ states. The total angular momentum projection $|\Omega|$ can then take the values $\frac{1}{2}$ and $\frac{3}{2}$. A unique state $|\Omega| = \frac{3}{2}$ originates from $^2\Pi(\Sigma = \pm\frac{1}{2}, \pm\Lambda = 1)$ state, while two states with $|\Omega| = \frac{1}{2}$ states originate from mixing of the $^2\Pi(\Sigma = \pm\frac{1}{2}, \Lambda = \mp 1)$ and $^2\Sigma^+(\Sigma = \pm\frac{1}{2}, \Lambda = 0)$ states. The Hamiltonian for the $|\Omega| = \frac{3}{2}$ state is trivially reduced to one element only, which can be written as $H(|\Omega| = \frac{3}{2}) = V(^2\Pi) + 2A_{\text{Rb}}$ and asymptotically corresponds to the $j = \frac{3}{2}$ state of the Rb atom. For the $|\Omega| = \frac{1}{2}$ state the Hamiltonian can be written as

$$H(|\Omega| = \tfrac{1}{2}) = \begin{pmatrix} V(2\,^2\Sigma^+) & \sqrt{2}A_{\text{Rb}} \\ \sqrt{2}A_{\text{Rb}} & V(1\,^2\Pi) + A_{\text{Rb}} \end{pmatrix}. \tag{6}$$

Two eigenvalues of this matrix asymptotically correspond to both the $j = \frac{1}{2}$ and $\frac{3}{2}$ states of the excited Rb($5p$) atom.

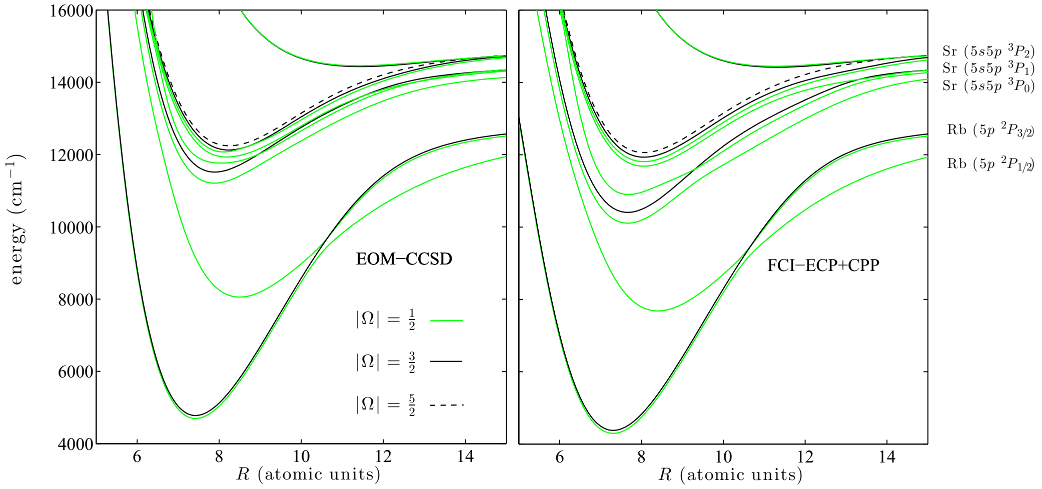

FIG. 8. (Color online) The EOM-CCSD potential energy curves of RbSr excited states including an atomic spin-orbit interaction as explained in the text resulting from the (a) EOM-CC approach and (b) FCI–ECP+CPP approach.

For the interaction of the ^3P state of Sr and the ^2S state of Rb the situation is somewhat more complicated. As we have mentioned in previous sections, the resulting dimer states for the Rb($5s\,^2S$)-Sr($5s5p\,^3P$) interaction in the Hund's case (a) are $^{2,4}\Sigma^+$ and $^{2,4}\Pi$. The possible quantum numbers for spin-orbit coupled states for that case are $|\Omega| = \frac{1}{2}, \frac{3}{2}$, and $\frac{5}{2}$. The maximal value of $|\Omega|$ corresponds trivially to the single state, namely, $H(|\Omega| = \frac{5}{2}) = V(1\,^4\Pi) + A_{\rm Sr}$ asymptotically corresponding to the metastable state of the Sr atom $^3P_2$. The $|\Omega| = \frac{3}{2}$ states can be obtained by coupling three states: $^4\Sigma^+(\Sigma = \pm\frac{3}{2}, \Lambda = 0)$, $^2\Pi(\Sigma = \pm\frac{1}{2}, \Lambda = \pm 1)$, and $^4\Pi(\Sigma = \pm\frac{1}{2}, \Lambda = \pm 1)$. The corresponding Hamiltonian from which we can obtain the Hund's (c) case representation reads

$$H\big(|\Omega| = \tfrac{3}{2}\big) = \begin{pmatrix} V(^2\Pi) + \frac{2}{3}A_{\rm Sr} & \sqrt{\frac{1}{3}}A_{\rm Sr} & -\frac{\sqrt{2}}{3}A_{\rm Sr} \\ \sqrt{\frac{1}{3}}A_{\rm Sr} & V(^4\Sigma^+) & \sqrt{\frac{2}{3}}A_{\rm Sr} \\ -\frac{\sqrt{2}}{3}A_{\rm Sr} & \sqrt{\frac{2}{3}}A_{\rm Sr} & V(^4\Pi) + \frac{1}{3}A_{\rm Sr} \end{pmatrix}. \tag{7}$$

Two of these states asymptotically correspond to the $^3P_2$ Sr state and one corresponds to the $^3P_1$ Sr state. Finally, for the $|\Omega| = \frac{1}{2}$ we have five states involved: $^2\Sigma^+(\Sigma = \pm\frac{1}{2}, \Lambda = 0)$, $^2\Pi(\Sigma = \mp\frac{1}{2}, \Lambda = \pm 1)$, $^4\Sigma^+(\Sigma = \pm\frac{1}{2}, \Lambda = 0)$, $^4\Pi(\Sigma = \mp\frac{1}{2}, \Lambda = \pm 1)$, and $^4\Pi(\Sigma = \pm\frac{3}{2}, \Lambda = \mp 1)$. The Hamiltonian that describes the coupled $|\Omega| = \frac{1}{2}$ states has the following form:

$$H(|\Omega| = \tfrac{1}{2}) = \begin{pmatrix} V(^2\Sigma^+) & \sqrt{\frac{8}{9}}A_{\rm Sr} & 0 & -\frac{1}{3}A_{\rm Sr} & \sqrt{\frac{1}{3}}A_{\rm Sr} \\ \sqrt{\frac{8}{9}}A_{\rm Sr} & V(^2\Pi) - \frac{2}{3}A_{\rm Sr} & \frac{1}{3}A_{\rm Sr} & -\frac{\sqrt{2}}{3}A_{\rm Sr} & 0 \\ 0 & \frac{1}{3}A_{\rm Sr} & V(^4\Sigma^+) & \sqrt{\frac{8}{9}}A_{\rm Sr} & \sqrt{\frac{2}{3}}A_{\rm Sr} \\ -\frac{1}{3}A_{\rm Sr} & -\frac{\sqrt{2}}{3}A_{\rm Sr} & \sqrt{\frac{8}{9}}A_{\rm Sr} & V(^4\Pi) - \frac{1}{3}A_{\rm Sr} & 0 \\ \sqrt{\frac{1}{3}}A_{\rm Sr} & 0 & \sqrt{\frac{2}{3}}A_{\rm Sr} & 0 & V(^4\Pi) - A_{\rm Sr} \end{pmatrix}. \tag{8}$$

The eigenstates of the Hamiltonian for $\Omega = \frac{1}{2}$ correspond to all components of the ^3P asymptote of the excited Sr atom: The lowest eigenvalue represents the interaction of the Rb atom with the $^3P_0$ state of Sr and two states correspond to the interaction with $^3P_1$ and two with $^3P_2$. The resulting spin-orbit coupled PECs are shown in Fig. 8. The EOM-CC and FCI–ECP+CPP approaches give very consistent potential energy curves, except for some of the states that correlate with the Rb($5s\,^2S$)+Sr($5s5p\,^3P_{0,1,2}$) asymptote, which originate from doublet $3\,^2\Sigma^+$ and $2\,^2\Pi$ states, which are about 20% deeper in the case of the FCI–ECP+CPP method.

For the Rb($5p\,^2P_{1/2,3/2}$)-Sr(^1S) manifold the $|\Omega| = \frac{1}{2}$ curves exhibit the avoided crossing where the $1\,^2\Pi$ and $2\,^2\Sigma^+$ states cross. Since the $1\,^2\Pi$ and $2\,^2\Sigma^+$ states are separated in energy by a much larger amount than the SO constant $A_{\rm Rb}$, they preserve their Hund's (a) case character over most of the internuclear distances in the chemical range. However, the corresponding bound levels may well be strongly coupled as is the case, for instance, in heavy alkali-metal dimers such as Rb$_2$ [86]. For the states that correlate with the Rb($5s\,^2S$)+Sr($5s5p\,^3P_{0,1,2}$) asymptote the character of Hund's case (c) states is drastically changed since the $2\,^2\Pi$

and $3\,^2\Sigma^+$, as well as $1\,^4\Pi$, states are much closer in energy. Therefore, these states are strong mixtures of doublet and quartet states. It is also clear from Fig. 8 that among the states that correlate with Rb($5s\,^2S$)+Sr($5s5p\,^3P_2$) there are states with $|\Omega| = \frac{1}{2}$ and $\frac{3}{2}$ of very strong $^4\Sigma^+$ character. Also, in view of such strong mixing, it is clear that the state $|\Omega| = \frac{1}{2}$ that correlates with the Sr atomic clock line will have a nonzero transition dipole moment at finite distances. Hence, the vibrational states supported by such a state might be accessible with dipole transitions.

V. CONCLUSION AND OUTLOOK

In this work we have explored theground and excited states of the RbSr molecule, which is a good candidate for a paramagnetic, polar molecule and subject to intense experimental study. A primary goal of this paper was to provide a calculation of potential energy curves for the RbSr curves and dipole moment matrix elements and a comparison between two *ab initio* methods: the FCI method with the use of an ECP and a CPP and the CC-theory-based methods used with a small effective core potential.

It is usually difficult to provide an error bound for the *ab initio* calculations, unless we deal with a small, few-electron system [87], for which it is possible to study the convergence pattern not only for a systematically increased Gaussian basis set but also for a number of excitations introduced to the electronic wave function. Hence, for such a complicated system as RbSr molecule application of two different methods provides a better starting point for further modeling of potential energy curves with the help of high-resolution spectroscopy experiments. The discrepancies in calculations of potential energy curves between the methods used in this paper are very small for the ground state, for the states correlating with Rb asymptotes, and for the quartet states correlating with the strontium asymptotes. A bit larger discrepancies have been obtained for the doublet states of Rb($5s\,^2S$)+Sr($5s5p\,^3P$) systems, although the equilibrium distances and harmonic constants are consistent. For the higher excited states the agreement is moderately good. Using both methods we have found very good agreement of the values of permanent dipole moments of the ground-state RbSr system as well as doublet Rb($5p\,^2P$)+Sr($5s^2\,^1S$) and Rb($5s\,^2S$)+Sr($5s5p\,^3P$) states: Interestingly enough, the permanent dipole moments of the excited states are very large.

Finally, we have obtained the transition dipole moments for the excitations from the ground electronic state to Rb($5p\,^2P$)+Sr($5s^2\,^1S$) and Rb($5s\,^2S$)+Sr($5s5p\,^3P$) states. Again, there is good agreement between the two approaches used in this paper. Interestingly enough, we have found that there are nonzero transition dipole moments from the ground state to the doublet Rb($5s\,^2S$)+Sr($5s5p\,^3P$) state. This means that the possibility of driving for the dipole transitions to the vibrational states is supported by the electronic states that correlate with strongly forbidden ^3P_J lines of the strontium atom.

ACKNOWLEDGMENTS

This work was supported in part by the National Science Foundation (Grant No. NSF PHY11-25915). R.G. acknowledges support from the Institut Francilien de Recherches sur les Atomes Froids. P.S.Ż. is grateful for the support of the Foundation for Polish Science Homing Plus Programme (Grant No. 2011-3/14) co-financed by the European Regional Development Fund and the computer time from the Wroclaw Centre for Networking and Supercomputing. The authors are also grateful to Florian Schreck and Benjamin Pasquiou for sparking our interest in the RbSr system.

[1] C. Chin, R. Grimm, P. Julienne, and E. Tiesinga, Rev. Mod. Phys. **82**, 1225 (2010).

[2] L. D. Carr and J. Ye, New J. Phys. **11**, 055009 (2009).

[3] O. Dulieu and C. Gabbanini, Rep. Prog. Phys. **72**, 086401 (2009).

[4] D. DeMille, Phys. Rev. Lett. **88**, 067901 (2002).

[5] A. Micheli, G. K. Brennen, and P. Zoller, Nat. Phys. **2**, 341 (2006).

[6] I. Bloch, J. Dalibard, and W. Zwerger, Rev. Mod. Phys. **80**, 885 (2008).

[7] J. Deiglmayr, A. Grochola, M. Repp, K. Mörtlbauer, C. Glück, J. Lange, O. Dulieu, R. Wester, and M. Weidemüller, Phys. Rev. Lett. **101**, 133004 (2008).

[8] K.-K. Ni, S. Ospelkaus, M. H. G. de Miranda, A. Pe'er, B. Neyenhuis, J. J. Zirbel, S. Kotochigova, P. S. Julienne, D. S. Jin, and J. Ye, Science **322**, 231 (2008).

[9] S. Ospelkaus, A. Pe'er, K.-K. Ni, J. J. Zirbel, B. Neyenhuis, S. Kotochigova, P. S. Julienne, J. Ye, and D. S. Jin, Nat. Phys. **4**, 622 (2008).

[10] M. Debatin, T. Takekoshi, R. Rameshan, L. Reichsoellner, F. Ferlaino, R. Grimm, R. Vexiau, N. Bouloufa, O. Dulieu, and H.-C. Naegerl, Phys. Chem. Chem. Phys. **13**, 18926 (2011).

[11] T. Takekoshi, M. Debatin, R. Rameshan, F. Ferlaino, R. Grimm, H.-C. Nägerl, C. R. Le Sueur, J. M. Hutson, P. S. Julienne, S. Kotochigova, and E. Tiemann, Phys. Rev. A **85**, 032506 (2012).

[12] C.-H. Wu, J. W. Park, P. Ahmadi, S. Will, and M. W. Zwierlein, Phys. Rev. Lett. **109**, 085301 (2012).

[13] S. Ospelkaus, K.-K. Ni, D. Wang, M. H. G. de Miranda, B. Neyenhuis, G. Quéméner, P. S. Julienne, J. L. Bohn, D. S. Jin, and J. Ye, Science **327**, 853 (2010).

[14] P. S. Żuchowski and J. M. Hutson, Phys. Rev. A **81**, 060703(R) (2010).

[15] J. J. Hudson, B. E. Sauer, M. R. Tarbutt, and E. A. Hinds, Phys. Rev. Lett. **89**, 023003 (2002).

[16] S. V. Alyabyshev, M. Lemeshko, and R. V. Krems, Phys. Rev. A **86**, 013409 (2012).

[17] R. Guérout, M. Aymar, and O. Dulieu, Phys. Rev. A **82**, 042508 (2010).

[18] P. S. Żuchowski, J. Aldegunde, and J. M. Hutson, Phys. Rev. Lett. **105**, 153201 (2010).

[19] M. H. Anderson, J. R. Ensher, M. R. Matthews, C. E. Wieman, and E. A. Cornell, Science **269**, 198 (1995).

[20] P. G. Mickelson, Y. N. Martinez, A. D. Saenz, S. B. Nagel, Y. C. Chen, T. C. Killian, P. Pellegrini, and R. Cote, Phys. Rev. Lett. **95**, 223002 (2005).

[21] S. B. Nagel, P. G. Mickelson, A. D. Saenz, Y. N. Martinez, Y. C. Chen, T. C. Killian, P. Pellegrini, and R. Côté, Phys. Rev. Lett. **94**, 083004 (2005).

[22] S. Stellmer, M. K. Tey, B. Huang, R. Grimm, and F. Schreck, Phys. Rev. Lett. **103**, 200401 (2009).

[23] S. Stellmer, B. Pasquiou, R. Grimm, and F. Schreck, Phys. Rev. Lett. **109**, 115302 (2012).

[24] S. Stellmer, R. Grimm, and F. Schreck, Phys. Rev. A **87**, 013611 (2013).

[25] S. Stellmer, M. K. Tey, R. Grimm, and F. Schreck, Phys. Rev. A **82**, 041602 (2010).

[26] M. K. Tey, S. Stellmer, R. Grimm, and F. Schreck, Phys. Rev. A **82**, 011608 (2010).

[27] G. Reinaudi, C. B. Osborn, M. McDonald, S. Kotochigova, and T. Zelevinsky, Phys. Rev. Lett. **109**, 115303 (2012).

[28] B. Pasquiou, A. Bayerle, S. M. Tzanova, S. Stellmer, J. Szczepkowski, M. Parigger, R. Grimm, and F. Schreck, Phys. Rev. A **88**, 023601 (2013).

[29] M. Okano, H. Hara, M. Muramatsu, K. Doi, S. Uetake, Y. Takasu, and Y. Takahashi, Appl. Phys. B **98**, 691 (2010).

[30] H. Hara, Y. Takasu, Y. Yamaoka, J. M. Doyle, and Y. Takahashi, Phys. Rev. Lett. **106**, 205304 (2011).

[31] A. H. Hansen, A. Khramov, W. H. Dowd, A. O. Jamison, V. V. Ivanov, and S. Gupta, Phys. Rev. A **84**, 011606 (2011).

[32] P. Zhang, H. R. Sadeghpour, and A. Dalgarno, J. Chem. Phys. **133**, 044306 (2010).

[33] G. Gopakumar, M. Abe, B. P. Das, M. Hada, and K. Hirao, J. Chem. Phys. **133**, 124317 (2010).

[34] L. K. Sørensen, S. Knecht, T. Fleig, and C. M. Marian, J. Phys. Chem. A **113**, 12607 (2009).

[35] N. Nemitz, F. Baumer, F. Münchow, S. Tassy, and A. Görlitz, Phys. Rev. A **79**, 061403 (2009).

[36] M. Borkowski, P. S. Żuchowski, R. Ciuryło, P. S. Julienne, D. Kędziera, L. Mentel, P. Tecmer, F. Münchow, C. Bruni, and A. Görlitz, Phys. Rev. A **88**, 052708 (2013).

[37] A. R. Allouche and M. Aubert-Frécon, J. Chem. Phys. **100**, 938 (1994).

[38] N. Boutassetta, A. R. Allouche, and M. Aubert-Frécon, Chem. Phys. **189**, 33 (1994).

[39] N. Boutassetta, A. R. Allouche, and M. Aubert-Frécon, Chem. Phys. **189**, 393 (1995).

[40] A. R. Allouche and M. Aubert-Frécon, Chem. Phys. Lett. **222**, 524 (1994).

[41] L. M. Russon, G. K. Rothschopf, M. D. Morse, A. I. Boldyrev, and J. Simons, J. Chem. Phys. **109**, 6655 (1998).

[42] M. Ivanova, A. Stein, A. Pashov, A. V. Stolyarov, H. Knöckel, and E. Tiemann, J. Chem. Phys. **135**, 174303 (2011).

[43] K. Pak, W. C. Ermler, C. W. Kern, and V. E. Bondybey, J. Cluster Sci. **2**, 19 (1991).

[44] M. M. Marino, W. C. Ermler, C. W. Kern, and V. E. Bondybey, J. Chem. Phys. **96**, 3756 (1992).

[45] F. H. Hall, P. Eberle, G. Hegi, M. Raoult, M. Aymar, O. Dulieu, and S. Willitsch, Mol. Phys. **111**, 2020 (2013).

[46] M. Aymar, R. Guérout, and O. Dulieu, J. Chem. Phys. **135**, 064305 (2011).

[47] S. Knecht, H. J. A. Jensen, and T. Fleig, J. Chem. Phys. **128**, 014108 (2008).

[48] S. Knecht, L. K. Sörensen, H. J. A. Jensen, T. Fleig, and C. M. Marian, J. Phys. B **43**, 055101 (2010).

[49] M. Krych, W. Skomorowski, F. Pawłowski, R. Moszynski, and Z. Idziaszek, Phys. Rev. A **83**, 032723 (2011).

[50] F. H. Hall, M. Aymar, M. Raoult, O. Dulieu, and S. Willitsch, Mol. Phys. **111**, 1683 (2013).

[51] See Supplemental Material at http://link.aps.org/supplemental/10.1103/PhysRevA.90.012507 for the potential energy curves obtained in this paper.

[52] W. Müller and W. Meyer, J. Chem. Phys. **80**, 3311 (1984).

[53] W. Müller, J. Flesch, and W. Meyer, J. Chem. Phys. **80**, 3297 (1984).

[54] M. Foucrault, P. Millié, and J. Daudey, J. Chem. Phys. **96**, 1257 (1992).

[55] M. Aymar and O. Dulieu, J. Chem. Phys. **122**, 204302 (2005).

[56] M. Aymar and O. Dulieu, Mol. Phys. **105**, 1733 (2007).

[57] A. R. Allouche and M. Aubert-Frécon, J. Chem. Phys. **136**, 114302 (2012).

[58] J. Deiglmayr, A. Grochola, M. Repp, O. Dulieu, R. Wester, and M. Weidemüller, Phys. Rev. A **82**, 032503 (2010).

[59] M. Aymar, J. Deiglmayr, and O. Dulieu, Can. J. Phys **87**, 543 (2009).

[60] A. Kruzins, I. Klincare, O. Nikolayeva, M. Tamanis, R. Ferber, E. A. Pazyuk, and A. V. Stolyarov, Phys. Rev. A **81**, 042509 (2010).

[61] I. S. Lim, H. Stoll, and P. Schwerdtfeger, J. Chem. Phys. **124**, 034107 (2006).

[62] I. S. Lim, P. Schwerdtfeger, B. Metz, and H. Stoll, J. Chem. Phys. **122**, 104103 (2005).

[63] P. J. Knowles, C. Hampel, and H. J. Werner, J. Chem. Phys. **99**, 5219 (1993).

[64] H.-J. Werner, P. J. Knowles, G. Knizia, F. R. Manby, M. Schütz, *et al.*, MOLPRO, version 2012.1: a package of *ab initio* programs, 2012, see http://www.molpro.net

[65] J. F. Stanton and R. J. Bartlett, J. Chem. Phys. **98**, 7029 (1993).

[66] A. I. Krylov, Annu. Rev. Phys. Chem. **59**, 433 (2008).

[67] J. Stanton, J. Gauss, M. Harding, P. Szalay, *et al.*, CFOUR, a quantum chemical program package, http://www.cfour.de

[68] T. Helgaker, W. Klopper, H. Koch, and J. Noga, J. Chem. Phys. **106**, 9639 (1997).

[69] W. Skomorowski, R. Moszynski, and C. P. Koch, Phys. Rev. A **85**, 043414 (2012).

[70] D. Pavolini, T. Gustavsson, F. Spiegelmann, and J.-P. Daudey, J. Phys. B **22**, 1721 (1989).

[71] J. Deiglmayr, M. Aymar, R. Wester, M. Weidemüller, and O. Dulieu, J. Chem. Phys. **129**, 064309 (2008).

[72] P. S. Żuchowski, M. Kosicki, M. Kodrycka, and P. Soldán, Phys. Rev. A **87**, 022706 (2013).

[73] B. Friedrich and D. Herschbach, Phys. Rev. Lett. **74**, 4623 (1995).

[74] M. Tomza, W. Skomorowski, M. Musial, R. González-Frez, C. P. Koch, and R. Moszynski, Mol. Phys. **111**, 1781 (2013).

[75] R. González-Férez and C. P. Koch, Phys. Rev. A **86**, 063420 (2012).

[76] M. Theis, G. Thalhammer, K. Winkler, M. Hellwig, G. Ruff, R. Grimm, and J. H. Denschlag, Phys. Rev. Lett. **93**, 123001 (2004).

[77] R. Ciuryło, E. Tiesinga, and P. S. Julienne, Phys. Rev. A **71**, 030701 (2005).

[78] S. Blatt, T. L. Nicholson, B. J. Bloom, J. R. Williams, J. W. Thomsen, P. S. Julienne, and J. Ye, Phys. Rev. Lett. **107**, 073202 (2011).

[79] B. Jeziorski, M. Bulski, and L. Piela, Int. J. Quantum Chem. **10**, 281 (1976).

[80] J. Jiang, Y. J. Cheng, and J. Mitroy, J. Phys. B **46**, 125004 (2013).

[81] O. Docenko, M. Tamanis, R. Ferber, T. Bergeman, S. Kotochigova, A. V. Stolyarov, A. de Faria Nogueira, and C. E. Fellows, Phys. Rev. A **81**, 042511 (2010).

[82] M. Tomza, F. Pawlowski, M. Jeziorska, C. P. Koch, and R. Moszynski, Phys. Chem. Chem. Phys. **13**, 18893 (2011).

[83] M. Tomza, M. H. Goerz, M. Musiał, R. Moszynski, and C. P. Koch, Phys. Rev. A **86**, 043424 (2012).

[84] W. Skomorowski, F. Pawłowski, C. P. Koch, and R. Moszynski, J. Chem. Phys. **136**, 194306 (2012).

[85] J. Van Vleck, Phys. Rev. **33**, 467 (1929).

[86] C. Amiot, O. Dulieu, and J. Vergès, Phys. Rev. Lett. **83**, 2316 (1999).

[87] M. Przybytek and B. Jeziorski, J. Chem. Phys. **123**, 134315 (2005).